The rotation-torsion spectrum of CD2HOH

Laurent H. Coudert, R A Motiyenko, L Margulès, F Kwabia Tchana

The rotation-torsion spectrum of CD_2HOH

L. H. Coudert[a,*], R. A. Motiyenko[b], L. Margulès[b], F. Kwabia Tchana[c]

[a] *Université Paris-Saclay, CNRS, Institut des Sciences Moléculaires d'Orsay, 91405, Orsay, France*
[b] *Laboratoire de Physique des Lasers, Atomes et Molécules, UMR 8523 CNRS - Université Lille I, Bât. P5, 59655 Villeneuve d'Ascq Cedex, France*
[c] *Université de Paris and University Paris Est Creteil, CNRS, LISA, F-75013 Paris, France*

Abstract

New transitions are reported in the submillimeter wave, terahertz, and far-infrared rotation-torsion spectrum of doubly-deuterated methanol CD_2HOH. The newly assigned transitions allow us to spectroscopically characterize torsional states with $0 \leq K \leq 12$ and $0 \leq v_t \leq 2$. Three line position analyses are carried out. In the first one, restricted to rotation-torsion lines involving torsional states with $3 \leq K \leq 12$ and $v_t \leq 2$, rotational energies are evaluated with a $J(J+1)$ Taylor-type expansion for each torsional state. 4853 transitions were accounted for with a unitless standard deviation of 11.4. In the second analysis, 126 torsional subband centers are fitted to obtain refined torsional parameters including the hindering potential. In the third analysis, 5911 rotation-torsion transitions involving torsional states with $v_t \leq 2$, and $J \leq 26$ are reproduced with a unitless standard deviation of 3.2 using a four-dimensional rotation-torsion fitting Hamiltonian.

Keywords: CD_2HOH; internal rotation; rotation-torsion; asymmetrical methyl group; hindering potential; line-position analysis; submillimeter wave; terahertz; far-infrared; 4-dimensional model

1. Introduction

Internal rotation of an asymmetrical monodeuterated CH_2D methyl group has been spectroscopically investigated in monodeuterated methyl formate [1, 2], methanol [3–12], propene [13], and acetaldehyde [14–16]. In the case of monodeuterated methanol, a global analysis based on a four-dimensional rotation-torsion fitting Hamiltonian could be carried out [17]. Although internal rotation of a monodeuterated CH_2D methyl group is only quantitatively different from that of a doubly-deuterated CD_2H methyl group, the latter has been studied in fewer molecules. The microwave spectrum of doubly-deuterated methyl formate was analyzed [18] accounting for the internal rotation with an effective approach. Doubly-deuterated methanol CD_2HOH, first studied a long time ago, was more difficult to model. It was first spectroscopically investigated by Quade and coworkers [5–7, 19] using microwave spectroscopy and transitions involving torsional levels up to $K = 2$ and $v_t = 6$ were assigned. Later, new transitions were recorded in the microwave and far-infrared (FIR) domains [20–24] allowing us to spectroscopically characterize all torsional levels with $3 \leq K \leq 9$ and $v_t \leq 2$. Rotation-torsion transitions were analyzed approximating the rotational energy of each torsional state with a $J(J+1)$ Taylor-type expansion. Various torsional parameters, including the hindering potential, were also determined thanks to an analysis of the torsional subband centers [20]. However, unlike in the monodeuterated species CH_2DOH, no global analysis of the rotation-torsion spectrum with a rotation-torsion fitting Hamiltonian [17] could be carried out.

In this paper, new assignments are reported in the microwave and FIR spectra of CD_2HOH for rotation-torsion transitions involving torsional states with $0 \leq K \leq 12$. A satisfactory line position analysis restricted to the 4853 lines with $K \geq 3$ and $v_t \leq 2$ is carried out. Improved torsional parameters are retrieved fitting the 126 available torsional subband centers. More importantly, the four-dimensional rotation-torsion fitting Hamiltonian developed for the monodeuterated species [17]

*Corresponding author: laurent.coudert@universite-paris-saclay.fr

is slightly modified and applied to the fitting of rotation-torsion transitions up to the e_1 torsional state and to $J = 26$, $K = 12$. This rotation-torsion fitting Hamiltonian was key to the assignment of rotation-torsion transitions involving torsional states with $K < 3$ as their rotational energy cannot be correctly evaluated with a Taylor-type expansion.

The paper has four remaining sections. In Section 2, the new assignments are reported and the results of the line position analysis for lines with $K \geq 3$ are given. Section 3 deals with the analysis of the torsional subbands centers and Section 4 with the global analysis of the rotation-torsion transitions. Section 5 is the discussion.

2. Assignments and analysis for $K \geq 3$

The spectra used in the present work have been described in our previous investigation [20]. They consist of millimeter wave (MM) and submillimeter wave (SMM) spectra recorded from 80 to 600 GHz and of terahertz (THZ) spectra spanning the range 0.7–1.52 THz. FIR Fourier transform spectra measured in the 19–670 cm^{-1} region were also used. The frequencies measured in the MM and SMM domains are characterized by an experimental uncertainty of 30 kHz. In the THZ domain, the uncertainty is 30 kHz below 1 THz and 50 kHz above. For FIR spectra, an experimental uncertainty of 0.3×10^{-3} cm^{-1} was adopted.

Torsional levels are labeled using either the scheme of Su and Quade [4] or that of El Hilali *et al.* [11]. The former makes use of the rotational quantum number K, with $K \geq 0$, and of the torsional label L. This label, denoted gn, consists of the letter g, either e or o, and of the positive integer n which is a counter. $g = e$ (o) indicates that the torsional function correlates with an even (odd) torsional function for $K = 0$. The scheme of El Hilali *et al.* [11] requires the same rotational quantum number K and the torsional quantum number v_t. A cross reference table between both schemes is given in Table 1 of our previous investigation [20]. In this investigation, rotation-torsion energy levels are assigned using four quantum numbers J, K, p, v_t, where p is an integer equal to 1 or 2, related to the C_s symmetry species of the level, allowing us to distinguish the two members of an asymmetry doublet. For the $|J, K, v_t, \pm\rangle$ rotation-torsion basis set wavefunctions defined in Eqs. (26) and (27) of Lauvergnat *et al.* [10], the quantum number p is defined as follows. For $K > 0$, p is 1 and 2 when $\pm(-1)^K$ is $+1$ and -1, respectively; for $K = 0$, $p = 1$ (2) when the torsional function is an even (odd) function of the torsional angle. This result is consistent with a $p = 1$ ($p = 2$) rotation-torsion energy level belonging to the C_s symmetry species A' (A'') for J even and A'' (A') for J odd.

The quantum number p is used instead of the usual asymmetric-top quantum numbers JK_aK_c because there is no straightforward way to assign in terms of K_c the rotation-torsion levels corresponding to the $|J, K_a, v_t, +\rangle$ and $|J, K_a, v_t, -\rangle$ rotation-torsion wavefunctions. This is due to the slight asymmetry of CD_2HOH, to the large amplitude torsional motion, and to the dependence of the inertia tensor on the angle of internal rotation. Symmetry considerations [10] allow us to derive the electric dipole selection rules for the quantum number p. For $\Delta J = 0$ we have $1 \leftrightarrow 2$ and for $\Delta J = 1$ $1 \leftrightarrow 1$ and $2 \leftrightarrow 2$.

The Taylor-type expansion used to compute the rotational energy for a given K, v_t torsional state, based on that of Fisher *et al.* [25], is expressed with the help of the rotational quantum number p as

$$E(J, K, p, v_t) = \sum_{m \geq 0} a_m(K, v_t)[J(J+1)]^m \pm \tfrac{1}{2} W(J, K, v_t) \quad (1)$$

where $a_m(K, v_t)$ are expansion parameters; the upper (lower) sign is for $p = 1$ (2); and $W(J, K, v_t)$ is the asymmetry splitting written

$$W(J, K, v_t) = \frac{(J+K)!}{(J-K)!}\{S + T\,J(J+1) + U\,[J(J+1)]^2 + V\,[J(J+1)]^3\} \quad (2)$$

where S, T, U, and V are expansion parameters depending on K, v_t. As already stressed in our previous investigation [20], in the case of CD_2HOH, the Taylor-type expansion of Eq. (1) allows us to satisfactorily reproduce rotational energies of torsional states with $K \geq 3$. It fails for $K < 3$ because for such low K-values the levels are close together and the effects of Hamiltonian operators with $\Delta K = 1$ matrix elements become important. Equation (1) of Ref. [17], where the zeroth-order rotation-torsion Hamiltonian is expressed in terms of the inverse generalized inertia tensor [26, 27], emphasizes that coupling terms with $\Delta K = 1$ matrix elements include Coriolis coupling terms of the form $\{P_\alpha, \mu(\alpha)_{\alpha,x}\}P_x$ and $\{P_\alpha, \mu(\alpha)_{\alpha,y}\}P_y$ and asymmetry terms in $\{P_x, P_z\}\mu(\alpha)_{x,z}$ and $\{P_y, P_z\}\mu(\alpha)_{y,z}$.

Perpendicular $K', v_t' \leftarrow K'', v_t''$ torsional subbands with $K', K'' \geq 3$ and $v_t', v_t'' \leq 2$ were reported in our previous investigation [20]. For some of them, additional transitions could be assigned extrapolating to higher-J values with the Taylor-type expansion. New subbands were also observed making use of the four-dimensional rotation-torsion approach. Figure 1, where the assigned torsional subbands are shown schematically, should be compared to Fig. 4 of our previous investigation [20]. New assignments were carried out for the $K = 10 \leftarrow 9$, $11 \leftarrow 10$, and $12 \leftarrow 11$ subbands with $v_t', v_t'' \leq 2$. Parallel transitions with $11 \leq K \leq 12$ and $v_t \leq 2$ were also observed for the first time. 72 torsional subbands could be assigned and the number of available parallel and perpendicular transitions, including those assigned in this work and those reported in Refs. [21, 23, 24], is 4853. These transitions were fitted simultaneously using the Taylor-type expansions of Eqs. (1) and (2). This analysis provides us with a means to verify the assignments since, as confirmed by Fig. 1, all torsional states are connected. Each transition was given a weight equal to the inverse of its experimental uncertainty squared. A total of 4853 transitions were analyzed with a unitless standard deviation of 11.4. Table 1 summarizes the results of the line position analysis for all subbands and for perpendicular transitions only. Most subbands display a satisfactory χ^2 close to 1. It is mainly for subbands characterized by low K-values equal of 3 or 4 that unsatisfactory large values of χ^2 tend to arise. Such torsional states, although much less perturbed than those with $K < 3$, are still coupled to neighboring states through interactions becoming important when J increases. Assignments, observed frequencies or wavenumbers, and observed minus calculated residuals are listed in Table S1 available in the supplemental material. The $a_m(K, v_t)$ expansion parameters of Eq. (1) and the S, T, U, and V parameters of Eq. (2) determined in the analysis are reported in Table 2 for $3 \leq K \leq 4$ and in Table S2 available in the supplemental material for all K-values. As emphasized by Table 2, the parameter $a_0(K = 3, v_t = 0)$ was set to zero as the lowest lying $K = 3, v_t = 0$ was used as reference state. The sign of the asymmetry parameter S is not constant. For $K = 3$, it is negative for $v_t = 0$ and 1, and positive for $v_t = 2$. For $v_t = 1$ it is negative for $K = 3$ and positive for $K = 4$. This further confirms that the rotational level assignment in terms of K_c is not straightforward.

Several subbands reported in our previous investigation [20] were reported almost at the same time by Mukhopadhyay [21–23]. The rotational assignments reported by this author in Tables 1 and 2 of Ref. [21] for the $K = 5, o_1 \leftarrow 4, e_1$ subband, for parallel transitions within the e_0, o_1, and e_1 torsional states, and for a few perpendicular transitions are only partially consistent with those in our previous investigation [20]. In Table 2 of Ref. [21], at least four lines are missassigned. The parallel transition at 333335.082 MHz does not belong to the $K = 3, e_1$ torsional state, but to $K = 3, o_1$; the parallel transition at 333163.863 MHz does not belong to $K = 7, o_1$ but to $K = 4, o_1$; the perpendicular transition at 353983.299 MHz is not a $J = 6 \leftarrow 7$ line, but a $J = 7 \leftarrow 8$; and the perpendicular transition at 312334.867 MHz does not belong to the $K = 6, e_1 \leftarrow 5, e_1$ torsional subband. The Q-branch origins given in Table 1 of Ref. [22], retrieved from the FIR spectrum recorded in this reference, are within ± 0.01 cm^{-1} from those listed in Table 6 of our previous investigation [20] for $K + 1, e_0 \leftarrow K, e_0$ torsional subbands with $3 \leq K \leq 8$. The wavenumbers given in Table 2 of Ref. [22] for the $K + 1, e_0 \leftarrow K, e_0$ torsional subbands with $6 \leq K \leq 8$ are within ± 0.002 cm^{-1} from those listed in the supplementary data associated with our previous investigation [20]. The two wavenumbers given in Table 2 of Mukhopadhyay [23] for the two lowest J-value lines of perpendicular subbands originating from K, e_0, with K ranging from 3 to 11, agree with the assignments reported in our previous investigation [20] and the present one. The $K = 4, o_1 \leftarrow 3, e_1$ torsional subband reported in Table 3 of Mukhopadhyay and Billinghurst [24] was already reported in our previous investigation [20].

3. Torsional spectrum analysis

The fitting torsional Hamiltonian used in the present investigation is the same as the one used in our previous investigation [20], except that additional distortion terms were used. The fitting torsional Hamiltonian, denoted H_t, depending on the torsional angle α and on the rotational quantum

Table 1: Results summary[a] of the torsional subbands[b] analysis

K	L	K	L	σ	N	J_{Max}	χ^2	K	L	K	L	σ	N	J_{Max}	χ^2
4	e_0	3	e_1	2.3361[c]	40	21	25.3	6	e_1	5	o_1	31.6227[c]	63	30	10.9
4	o_1	3	e_1	5.6743[d]	49	23	12.3	8	e_0	7	e_0	31.7347[d]	96	32	2.2
5	e_0	4	e_1	6.3685[c]	34	24	7.8	8	o_1	7	o_1	32.1139[c]	44	23	5.2
5	o_1	4	e_1	10.1700[d]	66	25	10.9	7	o_1	6	e_0	33.0705[c]	26	20	8.2
4	e_0	3	o_1	11.2172[d]	30	20	14.4	11	e_0	10	e_1	33.3657	28	24	0.6
4	o_1	3	o_1	14.5555[c]	39	16	11.4	10	o_1	9	e_1	33.5230	34	25	0.7
7	e_0	6	e_1	14.8732[c]	20	23	3.6	7	e_1	6	o_1	34.6759[c]	6	11	4.4
4	e_1	3	e_1	14.9047[c]	65	24	9.5	10	e_0	9	o_1	34.9181	56	34	0.8
4	e_0	3	e_0	15.0663[d]	44	17	60.5	6	e_1	5	e_0	35.4242[d]	72	31	1.2
6	o_1	5	e_1	15.3033[d]	102	29	7.3	9	o_1	8	o_1	35.7795[c]	84	31	0.7
5	e_0	4	o_1	15.5989[c]	42	18	11.2	9	e_1	8	e_1	36.0418[c]	46	23	4.8
4	o_1	3	e_0	18.4046[d]	49	17	57.2	9	e_0	8	e_0	36.1998[c]	78	30	2.2
5	e_1	4	e_1	18.8857[c]	78	25	7.7	11	o_1	10	e_1	36.7607	66	28	3.4
5	e_0	4	e_0	18.9371[d]	83	25	7.1	8	o_1	7	e_0	37.8802[c]	62	33	2.8
6	e_0	5	o_1	19.1917[c]	85	31	19.2	7	e_1	6	e_0	39.5032[d]	52	30	7.6
5	o_1	4	o_1	19.4004[d]	61	22	8.3	10	o_1	9	o_1	39.5785	54	24	0.8
7	o_1	6	e_1	20.6395[c]	52	21	1.6	11	e_0	10	o_1	40.3248	60	26	0.7
7	e_0	6	o_1	22.4769[c]	30	20	5.4	10	e_1	9	e_1	40.4822	72	28	1.3
5	o_1	4	e_0	22.7386[c]	22	20	8.3	10	e_0	9	e_0	40.6433	56	24	1.1
6	e_1	5	e_1	22.9069[d]	54	30	4.7	9	e_1	8	o_1	41.8350[c]	46	33	2.6
6	e_0	5	e_0	22.9932[d]	53	34	4.3	9	o_1	8	e_0	41.9250[c]	114	40	2.9
4	e_1	3	o_1	23.7859[c]	23	20	3.9	8	e_1	7	e_0	43.6734[c]	48	31	2.6
6	o_1	5	o_1	24.0190[d]	36	28	6.7	11	o_1	10	o_1	43.7198	38	29	2.0
9	e_0	8	e_1	24.2611[c]	44	22	0.8	11	e_1	10	e_1	44.6608	18	19	0.5
8	o_1	7	e_1	25.6812[c]	66	31	3.0	11	e_0	10	e_0	44.9852	52	36	1.2
8	e_0	7	o_1	25.9684[c]	76	31	8.1	10	o_1	9	e_0	45.3037	134	34	1.3
7	e_1	6	e_1	27.0722[c]	73	33	6.7	10	e_1	9	o_1	46.5376	30	24	0.5
7	e_0	6	e_0	27.3042[c]	74	30	5.5	9	e_1	8	e_0	47.9804[c]	68	30	1.4
4	e_1	3	e_0	27.6350[d]	19	17	39.7	12	o_1	11	o_1	48.3088	28	25	1.2
6	o_1	5	e_0	27.8205[d]	97	30	8.7	11	o_1	10	e_0	48.3802	98	35	1.3
5	e_1	4	o_1	28.1161[c]	43	18	4.4	12	e_1	11	e_1	48.6511	70	32	2.2
7	o_1	6	o_1	28.2432[c]	60	25	9.8	12	e_0	11	e_0	49.0378	66	29	1.1
10	e_0	9	e_1	28.8626	76	32	2.5	11	e_1	10	o_1	51.6199	40	21	1.4
9	e_0	8	o_1	30.0543[c]	100	35	1.6	12	o_1	11	e_0	51.7037	38	26	0.9
5	e_1	4	e_0	31.4544[c]	60	24	7.0	10	e_1	9	e_0	52.2628	20	21	0.8
8	e_1	7	e_1	31.4744[c]	62	32	1.7	12	e_1	11	o_1	56.5513	60	28	0.8

[a] The line position analysis of rotation-torsion transitions belonging to torsional subbands involving e_0, o_1, and e_1 torsional levels with $K \geq 3$ is described in Section 2.

[b] K and L for the upper and lower torsional levels, σ the subband center in cm^{-1}, N the number of assigned perpendicular transitions, J_{Max} the maximum J-value, and the unitless χ^2 are given for each torsional subband.

[c] Reported in our previous investigation [20].

[d] Reported in our previous investigation [20], additional transitions assigned in this work.

Table 2: Taylor-type expansion parameters determined in the torsional subbands[a] analysis

Parameter[b]	$K=3, e_0$	$K=3, o_1$	$K=3, e_1$
a_0		3.849112(13)	12.7302658(123)
a_1	0.69479101(57)	0.69467349(40)	0.69340586(16)
$a_2 \times 10^6$	3.850(9)	2.139(6)	−0.6357(11)
$a_3 \times 10^9$	−4.06(7)	−0.34(4)	0.013(3)
$a_4 \times 10^{12}$	18.46(21)	1.78(7)	0.3250(27)
$a_5 \times 10^{15}$	−29.249(243)		
$S \times 10^9$	−1.58(3)	−1.337(10)	0.4698(16)
$T \times 10^{12}$	−19.63(48)	−0.32(12)	0.10(1)
$U \times 10^{15}$	160.80(326)	−3.4(4)	−0.074(29)
$V \times 10^{18}$	−495.85(941)	4.2(5)	0.044(22)
$W \times 10^{21}$	568.00(981)		
Parameter[b]	$K=4, e_0$	$K=4, o_1$	$K=4, e_1$
a_0	15.0663474(116)	18.4045900(113)	27.6349712(118)
a_1	0.69480449(19)	0.69453481(21)	0.69340189(11)
$a_2 \times 10^6$	1.299(2)	0.3030(22)	−0.86596(72)
$a_3 \times 10^9$	−0.159(8)	−0.114(10)	0.0698(17)
$a_4 \times 10^{12}$	0.480(14)	0.044(21)	0.0932(14)
$a_5 \times 10^{15}$	−0.338(10)	0.065(15)	
$S \times 10^{12}$	−0.9969(85)	0.319(20)	0.0676(34)
$T \times 10^{15}$	0.32(7)	0.02(21)	0.010(21)
$U \times 10^{18}$	−0.75(22)	−0.5(8)	0.04(4)
$V \times 10^{21}$	1.9(3)	0.6(13)	−0.02(3)
$W \times 10^{24}$	−1.1(1)	−0.5(8)	

[a] Parameters determined in the torsional subband analysis described in Section 2 are listed. Each column corresponds to a torsional level labeled with K and L. Only parameters for $3 \leq K \leq 4$ are reported.

[b] Parameters, defined in Eqs. (1) and (2), are given in cm^{-1} and their uncertainty is given in parentheses in the same units as the last digit. A blank entry means that the parameter was set to 0.

number K, is expressed as

$$
\begin{aligned}
H_t &= \tfrac{1}{2} P_\alpha \mu(\alpha)_{\alpha,\alpha} P_\alpha + \tfrac{1}{2}\{P_\alpha, \mu(\alpha)_{\alpha,z}\} K \\
&+ \tfrac{1}{2}\{\mu(\alpha)_{z,z} - \tfrac{1}{2}[\mu(\alpha)_{x,x} + \mu(\alpha)_{y,y}]\} K^2 \\
&+ \sum_{i=1}^{6} V_i (1 - \cos i\alpha)/2 - D_{KK} K^4 \\
&+ k_1 P_\alpha K^3 + k_2 P_\alpha^2 K^2 + k_3 P_\alpha^3 K + k_4 P_\alpha^4 \\
&+ \sum_{i=1}^{6} V_{iK} (1 - \cos i\alpha) K^2 \\
&+ \sum_{i=1}^{6} V_{iK\alpha} \{P_\alpha, \cos i\alpha\} K + \sum_{i=1}^{6} V_{i\alpha\alpha} \{P_\alpha^2, \cos i\alpha\}
\end{aligned}
\tag{3}
$$

where $\mu(\alpha)_{\alpha,\alpha}$, $\mu(\alpha)_{\alpha,z}$, $\mu(\alpha)_{x,x}$, $\mu(\alpha)_{y,y}$, and $\mu(\alpha)_{z,z}$ are α-dependent components of $\boldsymbol{\mu}(\alpha)$ the generalized inverse inertia tensor [26, 27]; P_α is the momentum conjugated to α; $\{,\}$ is the anti-commutator; V_i, with $1 \le i \le 6$, are six zeroth-order potential energy parameters; and D_{KK}, k_1, k_2, k_3, k_4, V_{iK}, $V_{iK\alpha}$, $V_{i\alpha\alpha}$, with $1 \le i \le 6$, are 23 distortion parameters. The eight kinetic energy parameters involved in the generalized inverse inertia tensor are defined in Table I of Ref. [11]. These kinetic energy parameters and the parameters defined in Eq. (3) were fitted to the available torsional subband centers. The integers N and p_{Max} introduced in Ref. [10] for the calculation of the matrix elements of the generalized inverse inertia tensor components were respectively set to 11 and 9. The integer n_t, also defined in this reference, which is the maximum value of $|n|$ for the free internal rotation basis set functions $|n\rangle$, was set to 20. The data set includes the 6 torsional subbands involving torsional levels up to $K = 2$ and e_2 already considered [20]; the 72 subband centers retrieved in Section 2; and 46 subbands involving torsional levels with $v_t' > 2$. This last data set is almost identical to the one reported in Section 4.2 of our previous paper [20] except that the subbands $4, o_5 \leftarrow 3, e_5$ and $4, o_5 \leftarrow 3, e_2$ at respectively 232.28 and 654.69 cm^{-1} were added based on the rotational assignment reported by Mukhopadhyay [24]. The $7, e_3 \leftarrow 6, o_1$ subband was rotationally reassigned using the results of this reference and its band center decreased from 366.90 [20] to 366.74 cm^{-1} leading to a better agreement with its calculated value. The $1, o_5 \leftarrow 2, e_1$ and $3, o_5 \leftarrow 4, e_1$ subbands at respectively 715.60 and 773.06 cm^{-1} were also added using the wavenumbers reported by Mukhopadhyay and Billinghurst [24]. 4 subbands with no analysis of their rotational structure were removed from this last data set. Table S3 available in the supplemental material gives the observed minus calculated tables for the torsional subbands belonging to this last data set. Line position analyses were carried out for each subband using the $J(J+1)$ Taylor-type expansion of Section 2.

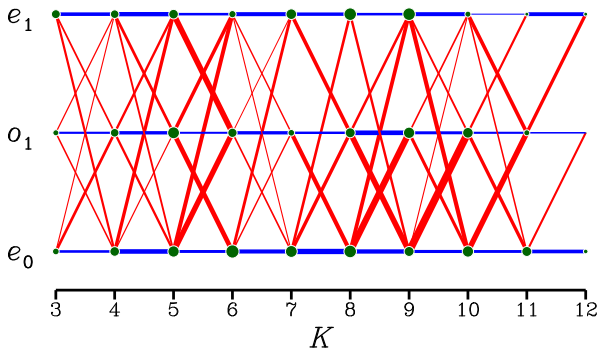

Figure 1: Transitions assigned in the MM, SMM, THZ, and FIR spectra for torsional levels with $3 \le K \le 12$ and $v_t \le 2$ are shown schematically. Torsional levels are indicated by a full circle with a diameter proportional to the number of parallel transitions. Solid lines indicate perpendicular transitions connecting different levels. Their width is proportional to the number of assigned transitions.

In the torsional spectrum analysis, weights equal to the inverse of the subband center uncertainty squared were used. For the 6 torsional subbands involving torsional levels up to $K = 2$ and e_2, an uncertainty of 0.02 cm^{-1} was assumed since there is no satisfactory analysis of their rotational structure. For the 72 subbands centers retrieved in Section 2, a smaller accuracy of 0.01 cm^{-1} was taken since their rotational structure was successfully analyzed. For the remaining subbands, a satisfactory analysis could not always be carried out and a larger experimental uncertainty of 0.1 cm^{-1} was assumed. Altogether, 126 torsional subbands were fitted. The kinetic energy parameters, involved in the generalized inverse inertia tensor, which were not varied were set to the value in Table 3 of our previous investigations [20]. Similarly, the zeroth-order potential energy parameters of Eq. (3) which were not varied were set to the value in Table 4 of Ref. [10]. Table 3 of the present paper lists the torsional subbands and the observed minus calculated residuals. The root mean square (RMS) value of the residuals is 0.048 cm^{-1}. The $0, e_2 \leftarrow 1, e_2$ subband, with a band center of 2.3 cm^{-1}, as retrieved from Ref. [6], could not be included in the data set because it displayed a too large observed minus cal-

culated residual of -0.17 cm^{-1}. For such low K- and v_t-values, such a large discrepancy may mean that this subband was missassigned in Ref. [6]. Table 4 reports the values of the fitted parameters. A comparison with the values in Table 5 of our previous paper [20] emphasizes that most parameters display small changes except the zeroth-order parameters I_x^0, V_1, and V_2. Concerning theses last two constants, the largest changes are displayed by the difference $V_1 - V_2$ while the sum $V_1 + V_2$ barely changes. The sum and difference are respectively -11.217 and -5.3415 cm^{-1}, with Table 5 of Ref. [20], and -11.317 and -4.573 cm^{-1} with Table 4 of the present papers.

4. Assignments for $K < 3$ and global analysis

The rotation-torsion transitions considered in this third analysis include those assigned in Section 2 and those involving at least one torsional state with $K < 3$. As stressed in Section 2, a $J(J+1)$ Taylor-type expansion is not appropriate to compute their rotational energy and assignment for these states were performed with the help of the 4-dimensional rotation-torsion approach. A preliminary fit of the transitions assigned in Section 2 and of those reported by Quade and coworkers [5–7, 19] and by Mukhopadhyay [21] was performed. From this fit parallel and perpendicular transitions characterized by a higher J-value were predicted and assigned. This bootstrap procedure was repeated until no more transitions could be found. Table 5 gives the number of parallel and perpendicular transitions thus assigned. Although the analysis carried out in Section 2 allowed us to check the assignments of transitions with $K \geq 3$, the assignment of the rotation-torsion transitions considered in this third analysis was further checked using 4-sided combination loops. All loops could be closed within experimental uncertainty when only unblended lines were involved. It should be emphasized that for all torsional states with $K < 3$, the maximum J-value and the transitions number are much higher than in the previous investigations [5–7, 19, 21].

The rotation-torsion Hamiltonian used in the present investigation differs slightly from the one introduced in Section III of Ref. [17]. Distortion effects were taken into account for the eight structural parameters, I_x^0, I_y^0, I_z^0, I_{xz}^0, I_x^1, I_α, I_x, and I_α^0, involved in the rotation-torsion Hamiltonian H_0 in Eq. (1) of Ref. [17]. These parameters are replaced by a $J(J+1)$ expansion so that that $P \rightarrow P + P_{JJ}J(J+1) + P_{JJJJ}[J(J+1)]^2$, where P is any of the eight structural parameters. Two rotation-torsion distortion operators were added, $P_\alpha P_x \mathbf{P}^2$ and $\{\sin\alpha, P_\alpha\}P_y$, with corresponding constants ρ_{xJ} and $\rho_{y\alpha}$.

In the analysis, energy levels were computed using the results of Section III C of Ref. [17]. The integers N, p_{Max}, and n_t, described in the previous section of this paper, were respectively set to 11, 9, and 22. The integers $v_{t\mathrm{Max}}$ and k_{Max}, describing respectively the number of torsional energies selected and the maximum value of $|k|$ in the rotation-torsion energy level calculation, were set to 18 and 15, respectively.

The fitted data set consists of 4335 microwave transitions and 1459 FIR transitions. 312 microwave and 10 FIR transitions were treated as unresolved doublets. The torsional subband centers fitted in Section 3 were also considered excluding those with $K < 3$ and $v_t \leq 3$. This amounts to 117 subband centers. A total of 5911 transitions were least squares fitted with a weight equal to the inverse of their uncertainty squared. For torsional subband centers, the uncertainty values are the same as in Section 3. The RMS of the observed minus calculated residuals is 0.135 MHz for microwave transitions, 0.21×10^{-3} cm^{-1} for FIR transitions, and 0.372 cm^{-1} for the torsional subband centers. The unitless standard deviation of the fit is 3.2. Tables S4, available in the supplementary material, gives the observed minus calculated table for the microwave and FIR rotation-torsion transitions.

The 95 parameters varied in the analysis are listed in Table 6 and include the eight structural parameters, their distortion coefficients, the six potential energy parameters, and the constants of the rotation-torsion distortion operators introduced Section III of Ref. [17] and in the present section. This table shows that the values obtained for the 6 kinetic energy parameters I_x^0, I_y^0, I_z^0, I_α, I_x, and I_α^0 are within a few percent from those calculated in Table 3 of our previous investigation [20]. For the two smaller parameters I_{xz}^0 and I_x^1, larger discrepancies arise. For the potential energy parameters V_1, V_2, V_3, and V_4, there is a satisfactory agreement with the values reported in Table 4 of Ref. [10], in Table 5 of our previous investigation [20] and in Table 4 of the present work. Values for the distortion parameters k_1, k_2, k_3, k_4, and D_K are also in some-

Table 3: Assignments,[a] observed subband centers,[b] and residuals[c] in the torsional spectrum of CD_2HOH

K	v_t	K	v_t	Obs	O−C	K	v_t	K	v_t	Obs	O−C	K	v_t	K	v_t	Obs	O−C
2	0	1	1	0.87(2)	−2	6	2	5	1	31.62(1)	0	11	5	10	2	284.75(10)	−7
1	2	2	1	1.30(2)	−2	8	0	7	0	31.73(1)	0	9	5	8	2	297.98(10)	−2
1	1	0	1	1.87(2)	0	8	1	7	1	32.11(1)	0	2	6	3	1	342.80(10)	3
1	0	0	0	2.23(2)	0	7	1	6	0	33.07(1)	−1	3	6	4	1	355.65(10)	0
1	2	0	2	2.26(2)	0	11	0	10	2	33.37(1)	1	3	6	4	0	358.99(10)	2
4	0	3	2	2.34(1)	0	10	1	9	2	33.52(1)	0	4	8	3	4	365.40(10)	6
0	1	1	0	3.92(2)	2	7	2	6	1	34.68(1)	1	7	6	6	1	366.74(10)	10
4	1	3	2	5.67(1)	2	10	0	9	1	34.92(1)	0	4	7	5	0	374.39(10)	11
5	0	4	2	6.37(1)	0	6	2	5	0	35.42(1)	0	6	6	5	1	375.45(10)	3
5	1	4	2	10.17(1)	1	9	1	8	1	35.78(1)	0	5	7	6	0	390.83(10)	0
4	0	3	1	11.22(1)	−2	9	2	8	2	36.04(1)	0	3	9	2	4	402.58(10)	8
4	1	3	1	14.56(1)	0	9	0	8	0	36.20(1)	0	6	7	7	0	408.80(10)	−1
7	0	6	2	14.87(1)	0	11	1	10	2	36.76(1)	−1	3	7	2	0	422.98(10)	−5
4	2	3	2	14.90(1)	0	8	1	7	0	37.88(1)	−1	7	7	8	0	427.61(10)	−7
4	0	3	0	15.07(1)	0	7	2	6	0	39.50(1)	0	2	7	1	0	440.94(10)	−3
6	1	5	2	15.30(1)	0	10	1	9	1	39.58(1)	0	8	8	9	0	447.17(10)	−16
5	0	4	1	15.60(1)	−1	11	0	10	1	40.32(1)	1	11	7	10	0	454.27(10)	7
4	1	3	0	18.40(1)	2	10	2	9	2	40.48(1)	0	1	7	0	0	459.79(10)	−5
5	2	4	2	18.89(1)	0	10	0	9	0	40.64(1)	0	1	9	0	4	468.51(10)	−11
5	0	4	0	18.94(1)	1	9	2	8	1	41.83(1)	0	10	7	9	0	472.05(10)	4
6	0	5	1	19.19(1)	0	9	1	8	0	41.93(1)	0	0	7	1	0	479.12(10)	−13
5	1	4	1	19.40(1)	−1	8	2	7	0	43.67(1)	0	0	8	1	0	479.92(10)	14
7	1	6	2	20.64(1)	−1	11	1	10	1	43.72(1)	−1	9	7	8	0	490.76(10)	−1
7	0	6	1	22.48(1)	1	11	2	10	2	44.66(1)	1	1	8	2	0	499.94(10)	−1
5	1	4	0	22.74(1)	1	11	0	10	0	44.99(1)	1	8	7	7	0	510.31(10)	−2
6	2	5	2	22.91(1)	0	10	1	9	0	45.30(1)	0	2	8	3	0	521.22(10)	0
6	0	5	0	22.99(1)	0	10	2	9	1	46.54(1)	0	3	8	4	1	540.15(10)	−1
4	2	3	1	23.79(1)	−2	9	2	8	0	47.98(1)	0	3	8	4	0	543.49(10)	1
6	1	5	1	24.02(1)	−1	12	1	11	1	48.31(1)	−2	4	9	5	1	566.03(10)	8
9	0	8	2	24.26(1)	0	11	1	10	0	48.38(1)	−1	2	10	3	3	567.03(10)	13
8	1	7	2	25.68(1)	−1	12	2	11	2	48.65(1)	1	5	8	4	1	570.99(10)	13
8	0	7	1	25.97(1)	1	12	0	11	0	49.04(1)	2	5	8	4	0	574.24(10)	7
7	2	6	2	27.07(1)	0	11	2	10	1	51.62(1)	1	4	8	3	1	591.70(10)	−13
7	0	6	0	27.30(1)	0	12	1	11	0	51.70(1)	−4	3	10	4	3	597.15(10)	10
4	2	3	0	27.63(1)	1	10	2	9	0	52.26(1)	0	4	9	3	1	599.94(10)	2
6	1	5	0	27.82(1)	0	6	4	5	3	53.09(10)	5	6	9	7	1	611.85(10)	4
5	2	4	1	28.12(1)	−1	12	2	11	1	56.55(1)	2	3	9	2	1	617.98(10)	−12
7	1	6	1	28.24(1)	0	5	4	4	3	59.95(10)	1	5	10	4	3	625.49(10)	1
10	0	9	2	28.86(1)	0	9	8	10	6	109.35(10)	2	4	11	5	3	626.13(10)	−3
9	0	8	1	30.05(1)	1	10	8	11	6	114.09(10)	7	4	10	3	3	654.69(10)	−5
5	2	4	0	31.45(1)	1	6	3	5	0	215.78(10)	−17	1	10	2	2	715.60(10)	−1
8	2	7	2	31.47(1)	0	4	10	3	9	232.28(10)	−15	3	10	4	2	773.06(10)	−4

[a] Torsional subbands are assigned using K and v_t for the upper and lower torsional levels.

[b] Subband centers are given in cm^{-1} in the column headed Obs. Their uncertainty is given in parentheses in 10^{-2} cm^{-1}.

[c] Observed minus calculated residuals are given in 10^{-2} cm^{-1} in the column headed O−C and correspond to the spectroscopic constants in Table 4.

Table 4: Parameters determined in the torsional subband center analysis

Parameter[a]	Value[b]	Parameter[a]	Value[b]
I_x^0	25.074(71)	V_3	370.687(83)
I_y^0	24.0877[c]	V_4	−0.7770[d]
I_z^0	6.0487(21)	V_5	0.0350[d]
I_{xz}^0	−0.0982[c]	V_6	−0.7460[d]
I_x^1	0.0157[c]	k_1	0.03441(54)
I_α	−1.1002[c]	k_2	−0.05300(78)
I_x	−1.0787[c]	k_3	0.03645(54)
I_α^0	5.2949(21)	k_4	−0.00948(15)
D_{KK}	0.00841(15)	V_{3K}	0.0141(16)
V_1	−7.947(46)	$V_{1\alpha\alpha}$	0.000682(60)
V_2	−3.369(50)		

[a] Torsional parameters are defined in Eq. (3).
[b] Kinetic energy parameters involved in the generalized inertia tensor are given in amu·Å^2. The remaining parameters are in cm^{-1}. Uncertainties are given in parentheses in the same units as the last digit.
[c] Constrained to the value in Table 3 of Ref. [20].
[d] Constrained to the value in Table 4 of Ref. [10].

what good agreement with those reported in these last two tables.

5. Discussion

New assignments were carried out in the spectrum of CD_2HOH. Compared to previous spectroscopic investigations [5–7, 19–21, 23, 24], assignments were extended to torsional states characterized by a higher K-values and to rotation-torsion transitions characterized by a higher J-values. A first analysis, reported in Section 2, was performed with the help of a $J(J+1)$ Taylor-type expansion for the limited set of transitions involving torsional states with $K \geq 3$. As the fitted data set includes a large number of parallel and perpendicular transitions allowing us to connect all observed torsional states, as emphasized by Fig. 1, this first analysis provides us with a means to verify the new assignments. It yielded 72 torsional subband centers which, along with those used in our previous investigation [20], were analyzed to retrieve various torsional parameters such as those describing the hindering potential. This second analysis is reported in Section 3 and allowed us to reproduce 126 subband centers with an RMS of 0.048 cm^{-1}. It should be

Table 5: Transitions assigned for $K < 3$ subbands[a]

K	L	N[b]	J_{Max}[b]	K	L	N[b]	J_{Max}[b]
0	e_0	20	24	1	e_1	31	22
0	o_1	20	24	2	e_0	28	21
0	e_1	19	23	2	o_1	33	24
1	e_0	37	24	2	e_1	29	23
1	o_1	36	23				
K	L		K	L		N[b]	J_{Max}[b]
1	e_0		0	e_0		28	25
1	e_0		0	o_1		31	20
1	e_0		0	e_1		29	22
1	o_1		0	e_0		36	22
1	o_1		0	o_1		15	23
1	o_1		0	e_1		6	23
1	o_1		1	e_1		11	19
1	e_1		0	e_0		27	21
1	e_1		0	o_1		19	20
1	e_1		0	e_1		25	20
2	e_0		1	e_0		44	22
2	e_0		1	o_1		51	22
2	e_0		1	e_1		60	19
2	o_1		1	e_0		43	22
2	o_1		1	o_1		47	23
2	o_1		1	e_1		23	22
2	e_1		1	o_1		47	24
2	e_1		1	e_1		62	19

[a] For parallel transitions, K and L are given for each torsional state. For perpendicular transitions, K and L are given for the upper and lower torsional levels.
[b] N and J_{Max} are respectively the number of assigned transitions and the maximum J-value for each torsional subband.

emphasized that in this second analysis, the 72 torsional subbands with $v_t \leq 2$ reported in Section 2 only involve torsional levels with $3 \leq K$. Torsional levels with $K < 3$ are found in the 46 torsional subbands involving torsional levels with $v'_t > 2$, reported in our previous paper [20], as well as in the 6 microwave torsional subbands, also reported in our previous paper, involving torsional levels with $K \leq 2$.

The main result of this investigation is the global analysis with the four-dimensional rotation-torsion fitting Hamiltonian developed for the monodeuterated species CH_2DOH [17]. This global analysis, reported in Section 4, was carried out up to $J = 26$ and $v_t = 2$ and observed frequencies and wavenumbers were reproduced with a unitless standard deviation of 3.2. Although, the rotation-torsion fitting Hamiltonian approach was key to the assignment of rotation-torsion transitions, especially those with $K < 3$, the value obtained for the unitless standard deviation is slightly too large. While somewhat satisfactory RMS values were obtained for the microwave and FIR data, it is for the torsional subband centers that an unsatisfactory RMS arises. Its value of 0.372 cm^{-1} is almost 10 times that retrieved in the analysis of Section 3. This stems from the large values of the torsional subband centers uncertainties compared to those of the microwave and FIR transitions. Inspection of the observed minus calculated table reveals that the largest residuals can be seen for torsional subbands involving high lying torsional levels with $v_t > 2$, not involved in the microwave and FIR data sets. It should be stressed that a global analysis of the microwave and FIR transitions only, without the torsional subband centers, was attempted but was not satisfactory.

The reason why the rotation-torsion fitting Hamiltonian approach does not allow us to reproduce the observed line positions satisfactorily is not understood yet. It should be pointed out that even though the inverse inertia tensor $\boldsymbol{\mu}(\alpha)$ displays larger variations with the torsional angle α in CH_2DOH than in CD_2HOH, the results of the global analysis for the former species were more satisfactory [17].

In the spirit of the reduced Hamiltonian derived by Watson for asymmetric top molecules [28–30], one may wonder if a similar reduction could be carried out for the rotation-torsion fitting Hamiltonian used in this work so as to achieve a more satisfactory analysis. In the case of molecules displaying internal rotation of a symmetrical methyl group, such a reduction is available [31, 32]. Unfortunately a similar reduction cannot be carried out for the present rotation-torsion fitting Hamiltonian. The first step of the reduction process [28–32] requires expanding the unreduced Hamiltonian as a series. In the case of the rotation-torsion used in this work, this is not possible since even the zeroth-order Hamiltonian, H_0 in Eq. (1) of Ref. [17], cannot be written as a sum of rotation-torsion operators times a spectroscopic parameter.

References

[1] L. Margulès, L. H. Coudert, H. Møllendal, J.-C. Guillemin, T. R. Huet, and R. Janečkovà, *J. Mol. Spectrosc.* **254** (2009) 55–68, doi:10.1016/j.jms.2008.12.007.

[2] L. H. Coudert, B. J. Drouin, B. Tercero, J. Cernicaro, J.-C. Guillemin, R. A. Motiyenko, and L. Margulès, *Astrophys. J.* **779** (2013) 119, doi:10.1088/0004-637X/779/2/119.

[3] C. Richard Quade and R. D. Suenram, *J. Chem. Phys.* **73** (1980) 1127–1131, doi:10.1063/1.440263.

[4] Chun Fu Su and C. Richard Quade, *J. Mol. Spectrosc.* **134** (1989) 290–296, doi:10.1016/0022-2852(89)90315-9.

[5] M. Liu and C. R. Quade, *J. Mol. Spectrosc.* **146** (1991) 252–263, doi:10.1016/0022-2852(91)90003-S.

[6] Chun Fu Su, Mujian Liu, and C. Richard Quade, *J. Mol. Spectrosc.* **149** (1991) 557–558, doi:10.1016/0022-2852(91)90310-7.

[7] C. R. Quade, M. Liu, I. Mukhopadhyay, and C. F. Su, *J. Mol. Spectrosc.* **192** (1998) 378–385, doi:10.1006/jmsp.1998.7719.

[8] I. Mukhopdhyay, D. S. Perry, Yun-Bo Duan, J. C. Pearson, S. Albert, R. A. H. Butler, E. Herbst, and F. C. DeLucia, *J. Chem. Phys.* **116** (2002) 3710–3717, doi:10.1063/1.1447218.

[9] I. Mukhopdhyay, *J. Mol. Struct.* **695–696** (2004) 357–365, doi:10.1016/j.molstruc.2003.12.013.

[10] D. Lauvergnat, L. H. Coudert, S. Klee, and M. Smirnov, *J. Mol. Spectrosc.* **256** (2009) 204–215, doi:10.1016/j.jms.2009.04.007.

[11] A. El Hilali, L. H. Coudert, I. Konov, and S. Klee, *J. Chem. Phys.* **135** (2011) 194309, doi:10.1063/1.3662468.

[12] John C. Pearson, Shanshan Yu, and Brian J. Drouin, *J. Mol. Spectrosc.* **280** (2012) 119–133, doi:10.1016/j.jms.2012.06.012.

[13] Jean Demaison, Norman C. Craig, Ranil Gurusinghe, Michael J. Tubergen, Heinz Dieter Rudolph, Laurent H. Coudert, Peter G. Szalay, and Attila G. Császár, *J. Phys. Chem. A* **121** (2017) 3155–3166, doi:10.1021/acs.jpca.7b01470.

[14] Paul H. Turner and A. Peter Cox, *Chem. Phys. Lett.* **42** (1976) 84–88, doi:10.1016/0009-2614(76)80556-8.

[15] Paul H. Turner, A. Peter Cox, and Judith A. Hardy, *J. Chem. Soc. Faraday Trans. 2* **77** (1981) 1217–1231, doi:10.1039/F29817701217.

[16] L. H. Coudert, L. Margulès, C. Vastel, R. Motiyenko, E. Caux, and J.-C. Guillemin, *A&A* **624** (2019) A70, doi:10.1051/0004-6361/201834827.

Table 6: Rotation-torsion spectroscopic parameters obtained in the global line position analysis

Parameter[a]		Value[b]		Parameter[a]		Value[b]	
I_x^0	H_0	24.475(2)		c_4	$P_\alpha\{P_z, {P_x}^2 - {P_y}^2\}$	5.85(8)	$\times 10^{-4}$
I_y^0	H_0	24.216(2)		D_{1xy}	$\sin\alpha\{P_x, P_y\}$	6.11(5)	$\times 10^{-4}$
I_z^0	H_0	6.00876(1)		D_{1yz}	$\sin\alpha\{P_y, P_z\}$	8.08(4)	$\times 10^{-2}$
I_{xz}^0	H_0	−9.8188[c]	$\times 10^{-2}$	$\rho_{y\alpha}$	$\{\sin\alpha, P_\alpha\}P_y$	−8.80(7)	$\times 10^{-2}$
I_x^1	H_0	9.25(13)	$\times 10^{-3}$	λ_v	$P_\alpha {P_z}^3 \mathbf{P}^2$	−1.30(3)	$\times 10^{-5}$
I_α	H_0	−1.2330(3)		k_{2j}	$P_\alpha{}^2 {P_z}^2 \mathbf{P}^2$	4.20(5)	$\times 10^{-5}$
I_x	H_0	8.09(32)	$\times 10^{-2}$	k_{3j}	$P_\alpha{}^3 P_z \mathbf{P}^2$	−4.46(3)	$\times 10^{-5}$
I_α^0	H_0	5.2551[c]		M_v	$P_\alpha{}^4 \mathbf{P}^2$	1.558(10)	$\times 10^{-5}$
I_{zJJ}^0	H_0	−3.26(4)	$\times 10^{-5}$	H_K	${P_z}^6$	−5.38(24)	$\times 10^{-6}$
I_{xzJJ}^0	H_0	−1.69(160)	$\times 10^{-6}$	H_{KJ}	${P_z}^4 \mathbf{P}^2$	−6.55(680)	$\times 10^{-8}$
I_{xJJ}^1	H_0	6.55(17)	$\times 10^{-7}$	H_{JK}	${P_z}^2 \mathbf{P}^4$	−2.96(11)	$\times 10^{-8}$
$I_{\alpha JJ}$	H_0	1.27(3)	$\times 10^{-5}$	H_J	$\mathbf{P}^6$	−1.57(25)	$\times 10^{-11}$
I_{xJJ}	H_0	−2.63(7)	$\times 10^{-5}$	h_K	$\{{P_z}^4, {P_x}^2 - {P_y}^2\}$	6.37(24)	$\times 10^{-8}$
I_{xJJJJ}^0	H_0	−2.23(13)	$\times 10^{-9}$	h_{KJ}	$\mathbf{P}^2\{{P_z}^2, {P_x}^2 - {P_y}^2\}$	−1.80(18)	$\times 10^{-9}$
I_{yJJJJ}^0	H_0	1.45(21)	$\times 10^{-9}$	h_J	$2\mathbf{P}^4({P_x}^2 - {P_y}^2)$	−2.47(22)	$\times 10^{-11}$
I_{xJJJJ}^1	H_0	−2.64(51)	$\times 10^{-11}$	G_3	$(1-\cos 3\alpha)({P_x}^2 - {P_y}^2)$	−6.84(11)	$\times 10^{-3}$
V_1	$(1-\cos\alpha)/2$	−9.193(10)		G_6	$(1-\cos 6\alpha)({P_x}^2 - {P_y}^2)$	2.98(5)	$\times 10^{-3}$
V_2	$(1-\cos 2\alpha)/2$	−3.310(10)		l_v	$P_\alpha P_z \mathbf{P}^4$	5.73(21)	$\times 10^{-8}$
V_3	$(1-\cos 3\alpha)/2$	370.629(8)		g_v	$P_\alpha{}^2 \mathbf{P}^4$	−2.74(11)	$\times 10^{-8}$
V_4	$(1-\cos 4\alpha)/2$	1.86(2)		k_{3jj}	$P_\alpha{}^3 P_z \mathbf{P}^4$	2.92(4)	$\times 10^{-10}$
V_5	$(1-\cos 5\alpha)/2$	3.5000[d]	$\times 10^{-2}$	k_{4jj}	$P_\alpha{}^4 \mathbf{P}^4$	−2.24(3)	$\times 10^{-10}$
V_6	$(1-\cos 6\alpha)/2$	−7.4600[d]	$\times 10^{-1}$	V_{1KKJJ}	$(1-\cos\alpha){P_z}^2 \mathbf{P}^2$	−1.10(2)	$\times 10^{-6}$
D_K	$-{P_z}^4$	7.66(5)	$\times 10^{-3}$	V_{2KKJJ}	$(1-\cos 2\alpha){P_z}^2 \mathbf{P}^2$	1.63(14)	$\times 10^{-7}$
D_{KJ}	$-{P_z}^2 \mathbf{P}^2$	1.22(1)	$\times 10^{-3}$	V_{3KKJJ}	$(1-\cos 3\alpha){P_z}^2 \mathbf{P}^2$	−1.935(2)	$\times 10^{-4}$
D_J	$-\mathbf{P}^4$	1.174(6)	$\times 10^{-6}$	V_{6KKJJ}	$(1-\cos 6\alpha){P_z}^2 \mathbf{P}^2$	4.498(3)	$\times 10^{-4}$
d_k	$-\{{P_z}^2, {P_x}^2 - {P_y}^2\}$	2.78(4)	$\times 10^{-4}$	H_{1KK}	$(1-\cos\alpha)\{P_x, {P_z}^3\}$	−4.97(51)	$\times 10^{-4}$
d_j	$-2\mathbf{P}^2({P_x}^2 - {P_y}^2)$	3.09(32)	$\times 10^{-8}$	H_{1JJ}	$(1-\cos\alpha)\{P_x, P_z\}\mathbf{P}^2$	−2.58(1500)	$\times 10^{-7}$
k_1	$P_\alpha {P_z}^3$	3.14(2)	$\times 10^{-2}$	D_{2yz}	$\sin 2\alpha\{P_y, P_z\}$	1.56(3)	$\times 10^{-3}$
k_2	$P_\alpha{}^2 {P_z}^2$	−4.84(3)	$\times 10^{-2}$	D_{3yz}	$\sin 3\alpha\{P_y, P_z\}$	2.19(4)	$\times 10^{-2}$
k_3	$P_\alpha{}^3 P_z$	3.31(2)	$\times 10^{-2}$	D_{2xz}	$(1-\cos 2\alpha)\{P_x, P_z\}$	−6.05(29)	$\times 10^{-4}$
k_4	$P_\alpha{}^4$	−8.49(5)	$\times 10^{-3}$	D_{3xz}	$(1-\cos 3\alpha)\{P_x, P_z\}$	−9.38(4700)	$\times 10^{-5}$
V_{1KK}	$(1-\cos\alpha){P_z}^2$	5.93(9)	$\times 10^{-3}$	D_{2xy}	$\sin 2\alpha\{P_x, P_y\}$	1.579(10)	$\times 10^{-3}$
V_{3KK}	$(1-\cos 3\alpha){P_z}^2$	1.47(2)	$\times 10^{-2}$	D_{3xy}	$\sin 3\alpha\{P_x, P_y\}$	−2.23(4)	$\times 10^{-3}$
V_{5KK}	$(1-\cos 5\alpha){P_z}^2$	−1.85(8)	$\times 10^{-3}$	V_{1KKKK}	$(1-\cos\alpha){P_z}^4$	1.65(5)	$\times 10^{-5}$
l_k	$P_\alpha {P_z}^5$	1.46(6)	$\times 10^{-5}$	V_{2KKKK}	$(1-\cos 2\alpha){P_z}^4$	−1.91(6)	$\times 10^{-5}$
k_{2k}	$P_\alpha{}^2 {P_z}^4$	−1.03(4)	$\times 10^{-5}$	V_{3KKKK}	$(1-\cos 3\alpha){P_z}^4$	−1.95(12)	$\times 10^{-5}$
k_{4B}	$P_\alpha{}^6$	1.10(5)	$\times 10^{-6}$	$V_{2KK\alpha\alpha}$	$\{1-\cos 2\alpha, P_\alpha{}^2 {P_z}^2\}$	−6.39(47)	$\times 10^{-4}$
V_{1JJ}	$(1-\cos\alpha)\mathbf{P}^2$	−7.82(8)	$\times 10^{-4}$	$V_{1\alpha\alpha}$	$\{1-\cos\alpha, P_\alpha{}^4\}$	−1.01(5)	$\times 10^{-3}$
V_{2JJ}	$(1-\cos 2\alpha)\mathbf{P}^2$	1.218(8)	$\times 10^{-3}$	c_{1j}	$2P_\alpha{}^2({P_x}^2 - {P_y}^2)\mathbf{P}^2$	2.02(21)	$\times 10^{-9}$
V_{3JJ}	$(1-\cos 3\alpha)\mathbf{P}^2$	9.98(93)	$\times 10^{-5}$	c_3	$2P_\alpha{}^4({P_x}^2 - {P_y}^2)$	−3.34(30)	$\times 10^{-8}$
V_{4JJ}	$(1-\cos 4\alpha)\mathbf{P}^2$	1.36(2)	$\times 10^{-3}$	G_{1j}	$(1-\cos\alpha)({P_x}^2 - {P_y}^2)\mathbf{P}^2$	5.30(150)	$\times 10^{-9}$
V_{5JJ}	$(1-\cos 5\alpha)\mathbf{P}^2$	−1.05(2)	$\times 10^{-3}$	G_{2j}	$(1-\cos 2\alpha)({P_x}^2 - {P_y}^2)\mathbf{P}^2$	1.36(9)	$\times 10^{-7}$
Δ_{xz}	$P_\alpha{}^2\{P_x, P_z\}$	−3.87(50)	$\times 10^{-4}$	G_{3j}	$(1-\cos 3\alpha)({P_x}^2 - {P_y}^2)\mathbf{P}^2$	1.44(3)	$\times 10^{-7}$
H_1	$(1-\cos\alpha)\{P_x, P_z\}$	−2.05(29)	$\times 10^{-3}$	L_{KKJ}	${P_z}^6 \mathbf{P}^2$	1.44(21)	$\times 10^{-12}$
δ_{xz}	$P_\alpha\{P_x, {P_z}^2\}$	9.13(100)	$\times 10^{-4}$	L_{KJ}	${P_z}^4 \mathbf{P}^4$	7.39(77)	$\times 10^{-12}$
ρ_{xJ}	$P_\alpha P_x \mathbf{P}^2$	−2.84(3000)	$\times 10^{-7}$	L_{JJK}	${P_z}^2 \mathbf{P}^6$	−1.84(2)	$\times 10^{-13}$
L_v	$P_\alpha P_z \mathbf{P}^2$	1.80(2)	$\times 10^{-3}$	L_J	$\mathbf{P}^8$	1.01(18)	$\times 10^{-15}$
G_v	$P_\alpha{}^2 \mathbf{P}^2$	−8.79(11)	$\times 10^{-4}$	l_k	$\{{P_z}^6, {P_x}^2 - {P_y}^2\}$	−1.19(2)	$\times 10^{-10}$
G_1	$(1-\cos\alpha)({P_x}^2 - {P_y}^2)$	−5.09(5)	$\times 10^{-4}$	l_{jk}	$\mathbf{P}^2\{{P_z}^4, {P_x}^2 - {P_y}^2\}$	2.67(29)	$\times 10^{-13}$
c_1	$2P_\alpha{}^2({P_x}^2 - {P_y}^2)$	−3.08(5)	$\times 10^{-4}$				

[a] Parameter constants and operators are described in Ref. [17] and in Section 4.

[b] Kinetic energy parameters involved in the exact Hamiltonian H_0 are given in amu·Å^2; the remaining parameters are in cm^{-1}. Uncertainties are given in parentheses in the same units as the last digit.

[c] Constrained to the value in Table 3 of Ref. [20].

[d] Constrained to the value in Table 4 of Ref. [10].

[17] L. H. Coudert, M. Zemouli, R. A. Motiyenko, L. Margulès, and S. Klee, *J. Chem. Phys.* **140** (2014) 064307, doi:10.1063/1.4864203.
[18] L. H. Coudert, L. Margulès, T. R. Huet, R. A. Motiyenko, H. Møllendal, and J.-C. Guillemin, *A&A* **543** (2012) A46, doi:10.1051/0004-6361/201219120.
[19] C. F. Su and C. Richard Quade, *J. Chem. Phys.* **90** (1989) 1396–1402, doi:10.1063/1.456656.
[20] M. Ndao, F. Kwabia Tchana, L. H. Coudert, R. A. Motiyenko, L. Margulès, J. Barros, L. Manceron, and P. Roy, *J. Mol. Spectrosc.* **326** (2015) 136–143, doi:10.1016/j.jms.2016.03.014.
[21] Indra Mukhopadhyay, *Infr. Phys. & Tech.* **75** (2016) 139–144, doi:10.1016/j.infrared.2015.12.022.
[22] Indra Mukhopadhyay, *Infr. Phys. & Tech.* **75** (2016) 193–201, doi:10.1016/j.infrared.2015.12.023.
[23] Indra Mukhopadhyay, *Infr. Phys. & Tech.* **76** (2016) 116–121, doi:10.1016/j.infrared.2016.01.002.
[24] Indranath Mukhopadhyay and B. E. Billinghurst, *Infr. Phys. & Tech.* **113** (2021) 103563, doi:10.1016/j.infrared.2020.103563.
[25] J. Fisher, G. Paciga, Li-Hong Xu, S. B. Zhao, G. Moruzzi, and R. M. Lees, *J. Mol. Spectrosc.* **245** (2007) 7–20, doi:10.1016/j.jms.2007.06.004.
[26] C. R. Quade and Chun C. Lin, *J. Chem. Phys.* **38** (1963) 540–550, doi:10.1063/1.1733692.
[27] J. V. Knopp and C. R. Quade, *J. Chem. Phys.* **48** (1968) 3317–3324, doi:10.1063/1.1669609.
[28] J. K. G. Watson, *J. Chem. Phys.* **46** (1967) 1935–1949, doi:10.1063/1.1840957.
[29] J. K. G. Watson, *J. Chem. Phys.* **48** (1968) 181–185, doi:10.1063/1.1667898.
[30] J. K. G. Watson, *J. Chem. Phys.* **48** (1968) 4517–4524, doi:10.1063/1.1668020.
[31] B. Kirtman, *J. Chem. Phys.* **37** (1962) 2516–2539, doi:10.1063/1.1733049.
[32] Kuniaki Nakagawa, Shozo Tsunekawa, and Takeshi Kojima, *J. Mol. Spectrosc.* **126** (1987) 329–340, doi:10.1016/0022-2852(87)90240-2.